Quantum reactive scattering in three dimensions: Using tangent-sphere coordinates to smoothly transform from hyperspherical to Jacobi regions

Gregory A. Parker,[a] Mark Keil, and Michael A. Morrison[b]
Department of Physics and Astronomy, University of Oklahoma, Norman, Oklahoma 73019-0225

Stefano Crocchianti
Departmento Di Chimica, Universitá di Perugia, Perugia, Italy

(Received 29 November 1999; accepted 14 March 2000)

Hyperspherical coordinates are well suited for treating rearrangement processes in the strong interaction region, and several different hyperspherical coordinates have been used successfully for quantum reactive scattering by various research groups. However, it is well known that asymptotically the appropriate set of coordinates (for a three particle system) are the three sets of Jacobi coordinates. In this paper we show how one can smoothly connect the hyperspherical coordinates in the rearrangement region to Jacobi coordinates in the nonrearrangement region using tangent-sphere coordinates. This procedure reduces the computational time required to solve the quantum Schrödinger equation and eliminates the need for numerical projection. To illustrate this method, we apply it to the $F+H_2 \rightleftharpoons HF+F$ reaction, comparing reaction probabilities to those from previous benchmark calculations based on a conventional formulation. © *2000 American Institute of Physics.* [S0021-9606(00)00622-X]

I. INTRODUCTION

Rearrangement and exchange processes are important in nuclear,[1,2] atomic,[3–5] and molecular scattering.[6–9] Accurate theoretical treatments of such processes are paramount to understanding many chemical, atomic, and nuclear physics problems, including three-body recombination rates for controlling limitations in Bose–Einstein condensation,[3,4,10] collision-induced dissociation and recombination for accurate treatment of chemical kinetics,[11] and studying isotopic anomalies of the upper atmosphere. They are also the key to calculating cross sections for muon and positron scattering[12] and for e2e processes.[13] Many numerical methods have been developed to study these processes. Prominent among these are techniques which use hyperspherical coordinates, the advantages of which have been long recognized in many contexts.[7]

In wave-function propagation methods for solving the scattering equations for rearrangement collisions, significant practical difficulties arise because different coordinate systems are appropriate to different regions of configuration space. When reactants are well separated, the set of internal coordinates most suited to their behavior are those of the Jacobi system. But when these constituents are in close proximity, hyperspherical coordinates are far better suited to describe their physics. The point at which the gap between the hyperspherical and Jacobi regions must be bridged is where there appear such difficulties as nonphysical coupling at large hyperradii, the need to use different bases in different sectors of the domain of the hyperradius, the need to propagate through the same region twice, and loss of unitarity of the *S* matrix. In this paper we describe how to use a third set of orthogonal coordinates—tangent sphere coordinates—to bridge this gap via a propagation variable that continuously and smoothly connects hyperspherical and Jacobi regions and therefore completely eliminates the need for algebraic or numerical matching procedures of any kind. In addition to obviating numerical problems, use of tangent sphere coordinates results in a savings of CPU time.

In Sec. II we outline the quantal scattering theory in hyperspherical and Jacobi coordinates. We also detail the use of tangent sphere coordinates to avoid the need to project the scattering function in hyperspherical coordinates onto its counterpart in Jacobi coordinates. In Sec. III we describe a step-by-step implementation of this procedure. Then in Sec. IV we apply this method to the $F+H_2 \rightleftharpoons HF+F$ reaction, assessing its accuracy and value by comparing present results to those from previous benchmark calculations based on conventional formulation. In Sec. V we conclude with a summary of essential points.

II. THEORY

In wave-function propagation scattering methods the goal is to propagate a single-variable (radial) scattering function through configuration space into the asymptotic region where one can extract the scattering (*S*) matrix by matching to known analytic boundary conditions. For rearrangement collisions, such methods must overcome the problem that the grouping of particles in the exit channel may differ from that in the entrance channel.[7] If, for example, the collision of an

[a]Electronic mail: parker@mail.nhn.ou.edu
[b]Electronic mail: morrison@mail.nhn.ou.edu

atom A and a diatom BC leads to an atom and a diatom, then three possible arrangements of the constituents A, B, and C are possible:

$$A+BC \rightarrow A+BC, \tag{1a}$$

$$\rightarrow B+AC, \tag{1b}$$

$$\rightarrow C+AB. \tag{1c}$$

To denote a particular arrangement of particles, we shall use indices τ for the atom of mass m_τ and $\tau+1$ and $\tau+2$ for the diatom of mass $m_{\tau+1}+m_{\tau+2}$. Thus for the entrance and exit channel arrangements in Eq. (1a), $\tau=$A, $\tau+1=$B, and $\tau+2=$C. Although we shall write in terms of atom-diatom collisions, the formulation presented here applies equally to rearrangement collisions (1) in any three-particle system. For example, in electron–hydrogen atom scattering, the projectile electron plays the role of the ''atom'' A, while the ''diatom'' is the target hydrogen atom consisting of proton B and bound electron C.

A. Jacobi coordinates

The set of internal coordinates that best describe the asymptotic behavior of the atom and diatom for a given arrangement τ are those of the Jacobi system JS_τ. For colinear motion, these coordinates reduce to Cartesian coordinates. We use mass-scaled Jacobi coordinates. Let $\mathbf{X}_\tau$ denote a position vector from the origin of a space-fixed coordinate system to particle τ. After separation of the center-of-mass motion, the Jacobi coordinates for the relative motion are defined as

$$\mathbf{R}_\tau=\mathbf{X}_\tau-\frac{m_{\tau+1}\mathbf{X}_{\tau+1}+m_{\tau+2}\mathbf{X}_{\tau+2}}{m_{\tau+1}+m_{\tau+2}}, \tag{2a}$$

$$\mathbf{r}_\tau=\mathbf{X}_{\tau+2}-\mathbf{X}_{\tau+1}. \tag{2b}$$

The vector $\mathbf{r}_\tau$ is the internuclear axis of the diatom, while $\mathbf{R}_\tau$ is a vector from the center-of-mass of the diatom to the atom τ.

The corresponding mass-scaled Jacobi coordinates $\mathbf{S}_\tau$ and $\mathbf{s}_\tau$ are scaled versions of $\mathbf{R}_\tau$ and $\mathbf{r}_\tau$, respectively,[14–16]

$$\mathbf{S}_\tau=d_\tau\mathbf{R}_\tau \quad \text{and} \quad \mathbf{s}_\tau=\frac{\mathbf{r}_\tau}{d_\tau}. \tag{3}$$

The dimensionless scaling factor is defined in terms of the three-body reduced mass,

$$\mu=\left(\frac{m_A m_B m_C}{M}\right)^{1/2}, \tag{4}$$

and the total mass of the system $M=m_A+m_B+m_C$, as

$$d_\tau=\left[\frac{m_\tau}{\mu}\left(1-\frac{m_\tau}{M}\right)\right]^{1/2}. \tag{5}$$

These coordinates for one arrangement τ are illustrated in Fig. 1.

The scale factors in Eq. (3) change the lengths of the position vectors but not their orientation. Thus the angle Θ_τ between mass-scaled Jacobi vectors $\mathbf{S}_\tau$ and $\mathbf{s}_\tau$ is

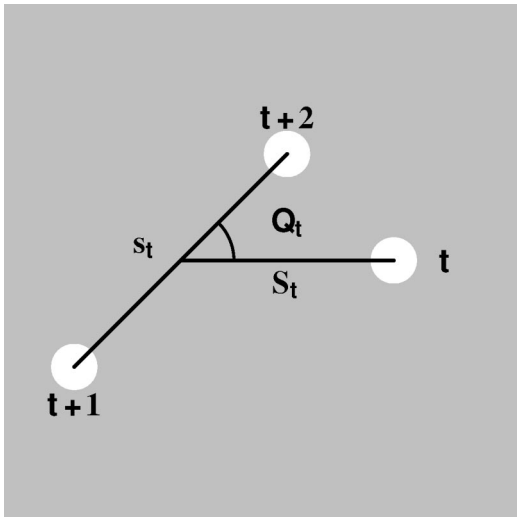

FIG. 1. Mass-scaled Jacobi coordinates $(S_\tau, s_\tau, \Theta_\tau)$ for an atom–diatom system.

$$\Theta_\tau=\cos^{-1}\left(\frac{\mathbf{S}_\tau\cdot\mathbf{s}_\tau}{S_\tau s_\tau}\right)=\cos^{-1}\left(\frac{\mathbf{R}_\tau\cdot\mathbf{r}_\tau}{R_\tau r_\tau}\right). \tag{6}$$

Physically, S_τ is the translational coordinate, which corresponds to the distance from the center-of-mass of the diatom to the atom, and s_τ is the vibrational coordinate, which corresponds to vibration (or dissociation) of the diatom. The angle Θ_τ corresponds to the orientation of the internuclear axis of the diatom with respect to the translational vector $\mathbf{S}_\tau$.

The three coordinates $(S_\tau, s_\tau, \Theta_\tau)$, which we shall call the internal coordinates, uniquely specify the center-of-mass position of the three particles in the plane defined by the system. To orient this plane in space, three additional angles—the three Euler angles—are required. Their effect is easily included in expansion bases using Wigner rotation matrices (see Sec. II F).[17] Our emphasis will be on the internal coordinates. For reactive collisions of the form (1), there are three sets of internal Jacobi coordinates. (The Faddeev approach[18,19] uses all three sets simultaneously.)

Mass-scaled Jacobi coordinates are convenient for two reasons. First, they yield an especially simple form for the kinetic energy operator, viz.[15,7]

$$T=-\frac{\hbar^2}{2\mu}(\nabla^2_{S_\tau}+\nabla^2_{s_\tau}). \tag{7a}$$

When written in terms of the rotational angular momentum $\mathbf{j}$ of the diatom and the orbital angular momentum $\mathbf{L}$ of the atom about the diatom, this expression assumes a form that is useful for conversion to other coordinate systems,

$$T=-\frac{\hbar^2}{2\mu}\frac{1}{S_\tau s_\tau}\left(\frac{\partial^2}{\partial S_\tau^2}+\frac{\partial^2}{\partial s_\tau^2}+\frac{1}{S_\tau^2}L_\tau^2+\frac{1}{s_\tau}j_\tau^2\right)S_\tau s_\tau. \tag{7b}$$

Second, transformations between mass-scaled Jacobi coordinates for different arrangements τ and τ' are effected by simple kinematic rotations of the form[7]

$$\begin{pmatrix}\mathbf{S}_{\tau'}\\ \mathbf{s}_{\tau'}\end{pmatrix}=\mathcal{R}(\chi_{\tau',\tau})\begin{pmatrix}\mathbf{S}_\tau\\ \mathbf{s}_\tau\end{pmatrix}. \tag{8a}$$

Here $\mathcal{R}$ is a 6×6 matrix which depends on the skew angle $\chi_{\tau',\tau}$ between arrangements τ and τ' as

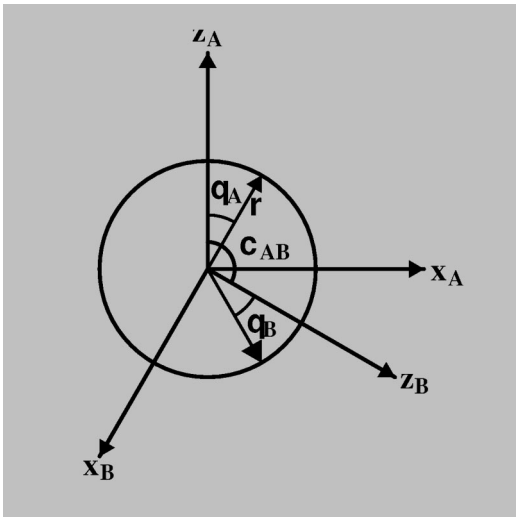

FIG. 2. Hyperspherical coordinates ρ and θ_τ in two dimensions and the skew angle χ_{AB} between the z_τ axes for arrangement channels τ=A and τ=B. Also shown is the hypercircle of radius ρ. The masses of the three constituent particles are taken to be equal, so all three skew angles are equal to $2\pi/3$.

$$\mathcal{R}(\chi_{\tau',\tau})=\begin{pmatrix} \cos(\chi_{\tau',\tau})\mathbf{I} & \sin(\chi_{\tau',\tau})\mathbf{I} \\ -\sin(\chi_{\tau',\tau})\mathbf{I} & \cos(\chi_{\tau',\tau})\mathbf{I} \end{pmatrix}, \tag{8b}$$

where $\mathbf{I}$ is the 3×3 unit matrix. The skew angle between adjacent arrangement channels τ and τ' is the negative obtuse angle defined by[7]

$$\cos\chi_{\tau',\tau}=-\frac{\mu}{d_\tau d_{\tau'} m_{\tau''}} \quad \text{and} \quad \sin\chi_{\tau',\tau}=-\frac{1}{d_{\tau'} d_\tau}, \tag{8c}$$

where $m_{\tau''}$ is the mass of the atom in the arrangement other than the two arrangements that define the skew angle. Thus for χ_{AB}, τ=A, τ'=B, and τ''=C; this angle is shown in Fig. 2. The skew angles obey the symmetry relations $\chi_{\tau,\tau}=0$ and $\chi_{\tau,\tau'}=-\chi_{\tau',\tau}$. The sum of all three skew angles must equal 2π

$$\sum_{\tau'} \chi_{\tau',\tau}=-2\pi \quad \text{and} \quad \sum_{\tau'} \chi_{\tau,\tau'}=+2\pi. \tag{9}$$

Note that τ, τ', and τ'' are cyclic permutations (A,B,C), (B,C,A), and (C,B,A).

B. Hyperspherical coordinates

Jacobi coordinates are not appropriate if the atom and diatom are in close proximity. In this region, the interactions among the particles are strong and rearrangements take place. More suitable for this rearrangement region are hyperspherical coordinates. A variety of hyperspherical coordinates are used in nuclear,[1,2] atomic,[3–5] and molecular scattering,[6–9] and one can easily transform from one hyperspherical coordinate system to another using rotational frame transformations, since all use the same hyperradius. Here we choose Delves hyperspherical coordinates,[15] which are particularly convenient for describing motion in each arrangement channel. For colinear motion, the Delves hyperspherical coordinates reduce to the usual plane polar coordinates.[6] [In practice, we begin propagating the scattering function in Adiabatically-adjusting Principal-axis Hyperspherical (APH) coordinates and transform to Delves coordinates at the outer boundary of the hyperspherical region.[7]]

For convenience, we choose the $x_\tau z_\tau$ plane and measure the angle θ_τ from the z_τ axis, as illustrated in Fig. 2. (From this point on, we assume that we have completed propagation in the three-dimensional hyperspherical region and the transformation from APH to Delves hyperspherical coordinates.) This angle and the hyperradius ρ are related to the JS_τ coordinates by

$$S_\tau=\rho\cos\theta_\tau \quad \text{and} \quad s_\tau=\rho\sin\theta_\tau. \tag{10}$$

In three dimensions, the internal rotation angle in HS_τ coordinates is Θ_τ; this angle is common to the JS_τ and HS_τ systems. Unlike the angles θ_τ and Θ_τ, the hyperradius ρ is independent of the arrangement τ, i.e.,

$$\rho=\sqrt{S_A^2+s_A^2}=\sqrt{S_B^2+s_B^2}=\sqrt{S_C^2+s_C^2}. \tag{11}$$

In principle, the domain of these coordinates is

$$0\leqslant\theta_\tau\leqslant\frac{\pi}{2}, \quad 0\leqslant\Theta_\tau\leqslant\pi, \quad 0\leqslant\rho<\infty. \tag{12a}$$

In practice, however, the values of ρ and θ_τ are limited in the nonrearrangement regions, as

$$0\leqslant\theta_\tau\leqslant\theta_\tau^{\max}, \quad 0\leqslant\Theta_\tau\leqslant\pi, \quad 0\leqslant\rho\leqslant\rho_{\max}\leqslant\rho_{\text{asy}}, \tag{12b}$$

where $\rho_{\max}$ is large enough to enclose all rearrangement processes, and ρ_{asy} is the hyperradius at which one projects onto Jacobi channel bases. Later in this section, we show how ρ_{asy} can be reduced to $\rho_{\max}$ by matching in tangent-sphere coordinates. (In the rearrangement region, $0\leqslant\theta_\tau<\theta_\tau^{\max}$ to allow for exchange of any two particles.) The value $\theta_\tau^{\max}$ is the angle at which the atom–diatom interaction potential becomes repulsive; the hyperradius $\rho_{\max}$ is the outer constant-ρ contour of the HS_τ region, beyond which we switch to another coordinate system. In general, $\theta_\tau^{\max}$ for two adjacent arrangement channels, such as τ=A and τ'=B in Fig. 2, is related to the skew angle by

$$\theta_\tau^{\max}+\theta_{\tau'}^{\max}\leqslant\chi_{\tau',\tau}. \tag{13}$$

In practice, we desire near equality in this equation, so adjacent hyperspherical regions touch at the maximum excursion of their respective polar angles.

The determination of $\rho_{\max}$ requires consideration of the point of contact between HS_τ and JS_τ regions. In Jacobi coordinates surfaces of constant vibrational coordinate s_τ are half-cylinders of radius s_τ, as shown in Fig. 3. The maximum radius $s_\tau^{\max}$ is determined by the vibrational wave function of the diatom in arrangement τ: the domain $0\leqslant s_\tau\leqslant s_\tau^{\max}$ must encompass the range of s_τ where this function is nonzero. These wave functions appear in the expansion bases for the system wave function, and it is important that there be no overlap of basis functions for adjacent arrangements; see Fig. 4. Since the maximum hyperradius for a given arrangement is tangent to the Jacobi cylinders, we must determine $\rho_{\max}$ for each arrangement so as to ensure that adjacent cylinders do not overlap. So, although strictly speaking the

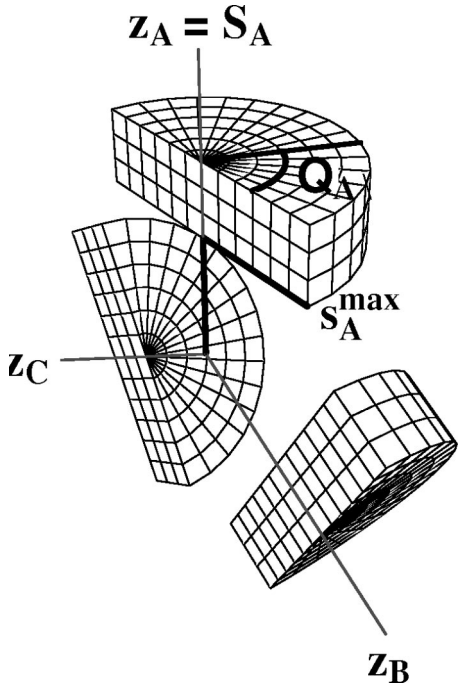

FIG. 3. Jacobi coordinates $(S_\tau, s_\tau, \Theta_\tau)$ for the three arrangement channels of an atom–diatom system with three equal masses. The translational propagation variable is S_τ, the vibrational coordinate is s_τ, and the angle between $\mathbf{S}_\tau$ and $\mathbf{s}_\tau$ is Θ_τ. Surfaces of constant s_τ are half-cylinders of radius s_τ, and surfaces of constant S_τ are half-planes normal to the z_τ axis.

hyperradii in Eq. (11) are independent of arrangement, in practice we obtain three different hyperradii, ρ_{AB}^{max}, ρ_{BC}^{max}, and ρ_{AC}^{max}. For example, for the adjacent regions shown (in the plane) in Fig. 2 we have

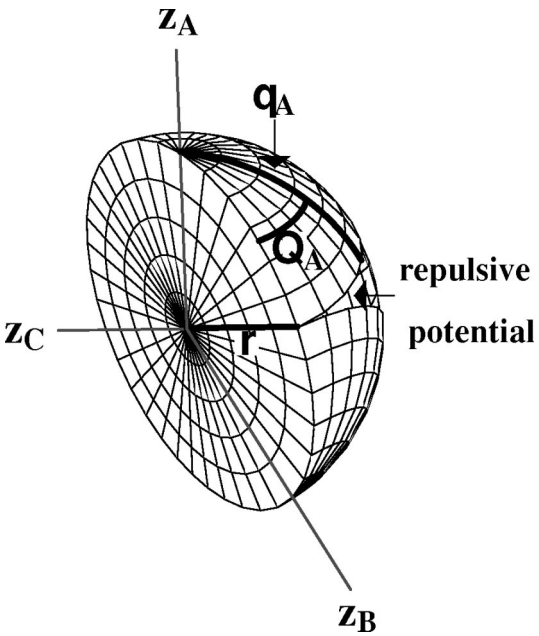

FIG. 4. Hyperspherical coordinates $(\rho, \theta_\tau, \Theta_\tau)$ for the three arrangement channels of an atom–diatom system with three equal masses. The translational propagation variable is the hyperradius ρ. The Delves hyperangle is θ_τ, and Θ_τ is the angle between the Jacobi vectors $\mathbf{S}_\tau$ and $\mathbf{s}_\tau$. The maximum values of the angles θ_τ are limited so as to exclude the repulsive potential region, here illustrated for arrangement channels τ=A and τ=B.

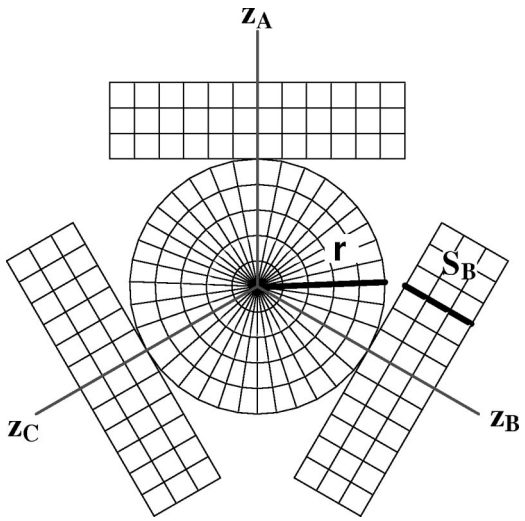

FIG. 5. A planar slice of the JS_τ and HS_τ systems for the three rearrangement channels of an atom–diatom system with three equal masses. The thick solid line indicates a possible trajectory for propagation of the scattering function into the asymptotic (Jacobi) region for channel τ=B. The gap between the hyperspherical and Jacobi regions arises because the hyperradius is tangent to the Jacobi contour of minimum S_τ at only one point. Procedures for bridging this gap are discussed in the text.

$$\rho_{AB}^{max} = \frac{1}{\sin \chi_{AB}} \sqrt{(s_A^{max})^2 + 2 s_A^{max} s_B^{max} \cos \chi_{AB} + (s_B^{max})^2}. \quad (14a)$$

(Here and in other figures, the coordinate labels x_τ, y_τ, and z_τ do not refer to the positions of the particles. Rather, they represent three orthogonal coordinates appropriate to the arrangement τ and the region under discussion. Thus, in JS_τ coordinates $z_\tau = S_\tau$, $x_\tau = s_\tau$, and $y_\tau = \Theta_\tau$.) To obtain a single outer boundary for all three HS_τ regions, we choose

$$\rho_{max} \equiv \max(\rho_{AB}^{max}, \rho_{BC}^{max}, \rho_{AC}^{max}). \quad (14b)$$

This choice leads to the lower bound on ρ in Eqs. (12b).

Equations for transforming between Jacobi and Delves hyperspherical coordinates are given in Table I. These are the familiar polar coordinate transformations, which can also be expressed as a conformal map. Volume elements for these systems, which are required for evaluation of matrix elements, appear in Table II.

Figure 4 shows the Delves HS_τ coordinates for τ=A for an atom–diatom system of three equal masses. Were we to include the full range of HS_τ coordinates, Eqs. (12a), the contours of constant ρ would be hemispheres of radius ρ. But in order to ensure zero overlap of vibrational wave functions in adjacent regions, we choose $\theta_\tau^{max} = \pi/3$. (In HS_τ coordinates, the vibrational distance is $\rho \sin \theta_\tau \approx \rho \theta_\tau$ for small polar angles θ_τ.) This choice excludes arrangements in which all three interparticle distances are large; here the potential $V(\rho, \theta_\tau, \Theta_\tau)$ is repulsive and the wave function for the system can be assumed to be zero.

C. Solving the scattering equation in Jacobi and hyperspherical coordinates

In scattering methods based on the close-coupling approximation, the many-body Schrödinger equation for the

TABLE I. Relationships between JS_τ, HS_τ, and TS_τ coordinates. The top entry in each block is the propagation variable; the bottom entry is the ''vibrational'' coordinate.

Region	Hyperspherical	Tangent sphere	Jacobi
Hyperspherical	$\rho=\rho$	$\rho=\sqrt{\frac{\rho_{\max}^2+w_\tau^2(1+v_\tau\rho_{\max})^2}{1+v_\tau^2w_\tau^2}}$	$\rho=\sqrt{S_\tau^2+s_\tau^2}$
	$\theta_\tau=\theta_\tau$	$\theta_\tau=\tan^{-1}\left[\frac{w_\tau}{v_\tau w_\tau^2+\rho_{\max}(1+v_\tau^2w_\tau^2)}\right]$	$\theta_\tau=\tan^{-1}\left(\frac{s_\tau}{S_\tau}\right)$
Tangent sphere	$v_\tau=\frac{\rho\cos\theta_\tau-\rho_{\max}}{\rho^2+\rho_{\max}^2-2\rho\,\rho_{\max}\cos\theta_\tau}$	$v_\tau=v_\tau$	$v_\tau=\frac{S_\tau-\rho_{\max}}{s_\tau^2+(S_\tau-\rho_{\max})^2}$
	$w_\tau=\frac{\rho^2+\rho_{\max}^2-2\rho\,\rho_{\max}\cos\theta_\tau}{\rho\sin\theta_\tau}$	$w_\tau=w_\tau$	$w_\tau=\frac{s_\tau^2+(S_\tau-\rho_{\max})^2}{s_\tau}$
Jacobi	$S_\tau=\rho\cos\theta_\tau$	$S_\tau=\frac{v_\tau w_\tau^2}{1+v_\tau^2w_\tau^2}+\rho_{\max}$	$S_\tau=S_\tau$
	$s_\tau=\rho\sin\theta_\tau$	$s_\tau=\frac{w_\tau}{1+v_\tau^2w_\tau^2}$	$s_\tau=s_\tau$

atom–diatom system is reduced to a set of coupled single-variable differential equations by expanding the system wave function in an appropriate basis.[20] The functions in this basis are constructed from complete sets in the relevant coordinates. In the JS_τ region, the basis for expansion of a wave function in the body-fixed reference frame consists of products of vibrational wave functions $\phi_{vj}^{(JS)}(s_\tau)$ for the diatom in arrangement τ and associated Legendre polynomials $P_j^\Lambda(\cos\Theta_\tau)$ for the rotational motion of the diatom. [For expansion in the space-fixed frame, the associated Legendre polynomials are replaced by coupled angular functions $\mathcal{Y}_{jl}^{JM}(\hat{S}_\tau,\hat{s}_\tau)$, where J and M are the quantum numbers for the total angular momentum $\mathbf{J}=\mathbf{j}+\mathbf{L}$ and its projection on the space-fixed z axis, and j and l are quantum numbers for $\mathbf{j}$ and $\mathbf{L}$.[20]

The resulting single-particle scattering equation must be propagated from the origin into the asymptotic region where matching to asymptotic boundary conditions yields the scattering matrix. For rearrangement collisions, this propagation encounters special problems owing to the use of different coordinate systems in different regions of configuration space. These problems are evident in Fig. 5, which shows a planar slice (colinear plane) through the JS_τ and HS_τ coordinates for all three arrangements of an equal-mass system. (The corresponding three-dimensional JS_τ and HS_τ contours appear in Figs. 3 and 4.) At the juncture between the JS_τ and HS_τ systems, the propagation variable changes from ρ to S_τ. For each arrangement τ, the hypersphere of radius $\rho_{\max}$ is tangent to the corresponding Jacobi contour of minimum S_τ at only one value of the vibrational coordinate, $\theta_\tau=s_\tau=0$. For any other angle θ_τ, there is a gap between the point $(\rho_{\max},\theta_\tau)$ and the start of the corresponding JS_τ region, $S_\tau^{(\min)}$. So if one knows the value of the scattering function on the surface of the hypersphere at $\rho_{\max}$, one knows the value at only a single point in the JS_τ region. Only at this point, therefore, can one determine the scattering function continuously from the HS_τ origin $\rho=0$ to an asymptotic value of the corresponding JS_τ translational coordinate S_τ.

To bridge the gap between the HS_τ and JS_τ regions, two strategies have been proposed so far.[7] (We shall propose a third in Sec. II D.) The most widely used approach is to match on the surface of the hypersphere of maximum radius.[7] A circle on this hypersphere is highlighted in Fig. 6; the actual matching surface is obtained by rotating this curve around each of the z_τ axes. In practice, rather than transform the scattering function at $\rho_{\max}$ to JS_τ coordinates and propagating further, one simply propagates in HS_τ coordinates from $\rho=0$ to a hypersphere of radius ρ_{asy} in the asymptotic region. There one projects the solution to JS_τ coordinates and matches to asymptotic boundary conditions in these coordinates (see Sec. II G). Of course, the value of ρ_{asy} must accommodate all angles θ_τ; i.e., this value must be in the asymptotic region for all required values of S_τ. This requirement results in a maximum hyperradius large enough that we just evaluate the JS_τ scattering function on the region of the sphere where the HS_τ and JS_τ systems now overlap, the cross-hatched region in Fig. 6.

Additional difficulties with this first procedure result from the dependence of the HS_τ vibrational basis functions

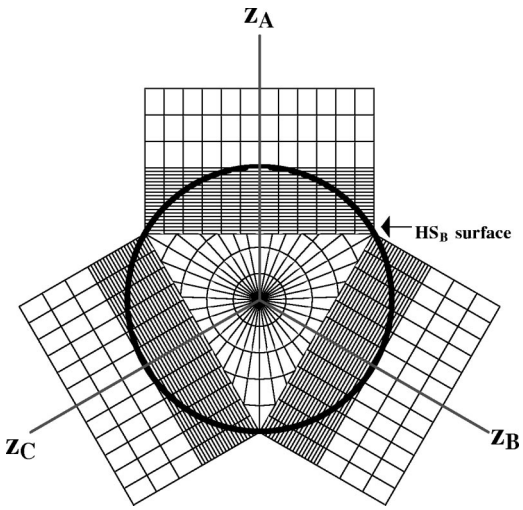

FIG. 6. One procedure for bridging the gap in Fig. 5. Solutions are matched to asymptotic boundary conditions in the region where the Jacobi cylinder overlaps with this hypersphere (cross-hatched region).

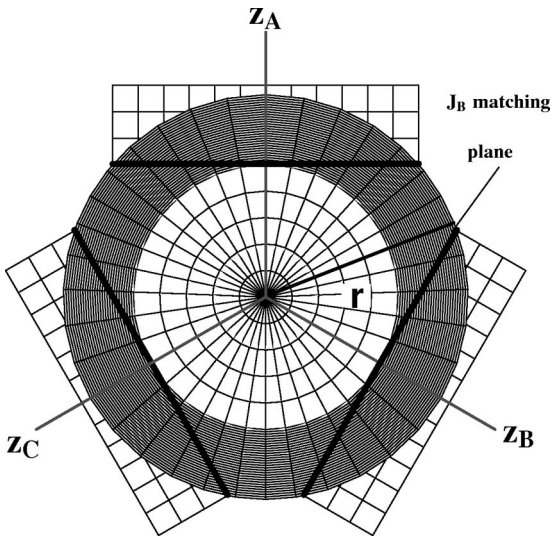

FIG. 7. An alternative to the scheme in Fig. 6 for bridging the gap in Fig. 5. One propagates the scattering function in HS_τ coordinates out to the planar surfaces of the Jacobi cylinders, shown by thick lines for all arrangement channels τ. One matches to solutions in Jacobi coordinates in the region where hypersphere overlaps these cylinders (cross-hatched region).

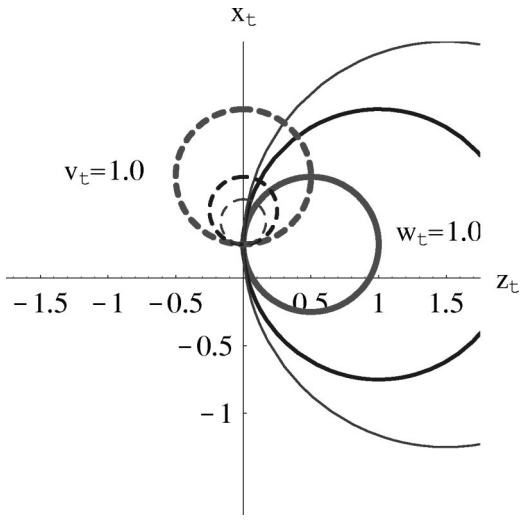

FIG. 8. Tangent sphere coordinates in two dimensions. For each coordinate v_τ (dashed curves) and w_τ (solid curves) we show three constant-coordinate contours: 1 (thick curves), 2, and 3 (thin curves).

on ρ, a consequence of the limited domain of the ''vibrational'' coordinate θ_τ in Eq. (12b). This dependence results in a nonphysical channel coupling at large hyperradii that requires the inclusion of basis functions for closed vibrational channels. Worse, it requires subdivision of the domain of the hyperradius into sectors, each of which has a different basis. One must therefore change bases at each sector boundary, a requirement that demands considerable memory and significant CPU time. Strategies for accommodating this demand are sector adiabatic bases,[7] diabatic by sector bases,[12] and smooth variable discretization.[21]

The second proposed way to bridge the gap between the HS_τ and JS_τ regions is to match scattering functions on Jacobi planes rather than on the hypersphere. This approach, illustrated in Fig. 7, entails propagating in HS_τ coordinates out to the JS_τ plane that corresponds to the minimum value of S_τ. On this plane, the HS_τ scattering function is matched to regular and irregular solutions that have been propagated inward from the asymptotic value of S_τ. In addition to the problems discussed in relation to matching on a hypersphere, this alternative suffers from the fact that, as shown in Fig. 7, the distance from the origin to the Jacobi matching plane depends on the hypersphere angle θ_τ. This dependence requires one to propagate through the cross-hatched region twice, outward in HS_τ coordinates where multiple hyperspherical sectors cross the boundary and inward in JS_τ coordinates. Moreover, this technique does not guarantee unitarity of the resulting S matrix; in fact, the extent to which the resulting S matrix violates unitarity varies with the scattering energy. Finally, it is not clear how to adapt this strategy to formulations based on variational methods, such as the Kohn variational method.[22] These difficulties have prompted our introduction of a third strategy based on tangent sphere coordinates.

TABLE II. Volume elements and are lengths along the propagation variable q_1 for the $JS_\tau(q_1=S_\tau)$, $TS_\tau(q_1=v_\tau)$, and $HS_\tau(q_1=\rho)$ coordinate systems.

Region	Volume element	Propagated arc length
Hyperspherical	$\frac{1}{4}\rho^5\sin^2(2\theta_\tau)d\rho\, d\theta_\tau\, d\hat{S}_\tau\, d\hat{s}_\tau$	$\rho_{\max}-\rho_{\min}$
Tangent sphere	$\dfrac{w_\tau^4(v_\tau w_\tau^2+\rho_{\max}+v_\tau^2 w_\tau^2\rho_{\max})^2}{(1+v_\tau^2 w_\tau^2)^6}\, dw_\tau dv_\tau d\hat{S}_\tau d\hat{s}_\tau$	$w_\tau\tan^{-1}\left(\dfrac{w_\tau}{2\rho_{\max}}\right)$
Jacobi	$S_\tau^2 s_\tau^2 dS_\tau\, ds_\tau\, d\hat{S}_\tau\, d\hat{s}_\tau$	$S_\tau^{(\max)}-S_\tau^{(\min)}$

D. Tangent sphere coordinates

Tangent sphere coordinates appear in the compendium of coordinate systems by Moon and Spencer.[23] (We have replaced their variable u by $1/w_\tau$ and v by v_τ; we have also shifted their coordinate z by $\rho_{\max}$.) For each arrangement τ, the TS_τ system is an orthogonal coordinate system whose coordinates $(v_\tau, w_\tau, \Theta_\tau)$ are related to rectangular coordinates by

$$(s_\tau)_x = x_\tau = \frac{w_\tau}{v_\tau^2 w_\tau^2+1}\cos\Theta_\tau, \tag{15a}$$

$$(s_\tau)_y = y_\tau = \frac{w_\tau}{v_\tau^2 w_\tau^2+1}\sin\Theta_\tau, \tag{15b}$$

$$S_\tau = z_\tau = \frac{v_\tau w_\tau^2}{v_\tau^2 w_\tau^2+1}+\rho_{\max}. \tag{15c}$$

Note that Θ_τ, the rotational angle of the diatom, is common to the TS_τ, JS_τ, and HS_τ systems.

The nature of these coordinates is most clear in the (x_τ, z_τ) plane obtained from Eqs. (15) by setting $\Theta_\tau=0$. In Fig. 8, curves of constant v_τ are circles of radius $-1/2v_\tau$ centered at $\rho_{\max}+1/2v_\tau$; these circles are tangent to a line parallel to the z_τ axis at $x_\tau=\rho_{\max}$. The contour $v_\tau=0$ is the x_τ axis. Similarly, curves of constant w_τ are circles that are tangent to the z_τ axis at $z_\tau=\rho_{\max}$. In the limit $w_\tau\to\infty$, these curves approach the z_τ axis.

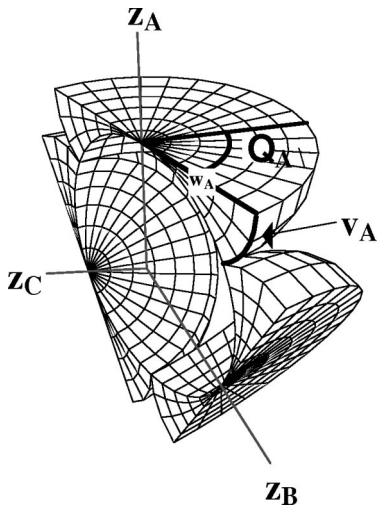

FIG. 9. Tangent sphere coordinates for the three arrangement channels of an atom–diatom system with three equal masses. The translational propagation variable is v_τ, the vibrational coordinate is w_τ, and the rotation angle about the z_τ axis is Θ_τ. Surfaces of constant v_τ are hemispheres, while surfaces of constant w_τ are half-toroids.

Constant-v_τ and constant-w_τ contours for three-dimensional TS_τ coordinates can be obtained by twirling the circles in Fig. 8 around the z axis. These coordinates are illustrated for an equal-mass sytem in Fig. 9. Strictly speaking the domains of the TS_τ coordinates are

$$0<w_\tau<\infty, \quad \text{and} \quad 0<v_\tau<\infty, \quad \text{and} \quad 0\leqslant\Theta_\tau\leqslant 2\pi. \tag{16}$$

These limits give for contours of constant v_τ spheres,

$$x_\tau^2+y_\tau^2+\left[z_\tau-\left(\rho+\frac{1}{2v_\tau}\right)\right]^2=\frac{1}{4v_\tau^2}, \tag{17a}$$

and for contours of constant w toroids about the origin (with no center opening),

$$x_\tau^2+y_\tau^2+(z_\tau-\rho)^2=w_\tau\sqrt{x_\tau^2+y_\tau^2}. \tag{17b}$$

But because only the domain $[0,\pi]$ is physically meaningful for the rotation angle Θ_τ, we restrict the maximum value of this variable to π. Hence the resulting surfaces are not closed. Surfaces of constant v_τ are now hemispheres, and surfaces of constant w_τ are half-toroids. (Additional restrictions must be imposed because of the proximity of the TS_τ system to the JS_τ and HS_τ systems, as we shall discuss below.) The coordinate origin is regained by setting $w_\tau=0$ and taking either limit $v_\tau\to\pm\infty$. The limit $w_\tau\to\infty$ is the z_τ axis, and $v_\tau=0$ corresponds to the half of the $x_\tau y_\tau$ plane for which $y_\tau>0$. To ensure that the tangent sphere region TS_τ will not overlap the HS_τ and JS_τ regions, the following limits should be used: $0<w_\tau<s_\tau^{\max}$, $-1/(2\rho_{\max})<v_\tau\leqslant 0$, and $0\leqslant\Theta_\tau^{\max}<\pi$.

E. Solving the scattering equation in tangent sphere coordinates

The tremendous advantage of TS_τ coordinates for rearrangement collisions is that they allow us to introduce a single propagation variable that varies continuously and smoothly from the origin (in the HS_τ region) to the asymptotic (JS_τ) region. Figure 10 illustrates such a propagation in the (x_τ,z_τ) plane, and Figs. 11 and 12 show the three-dimensional, three-arrangement analog. Beginning at the origin, the variable ρ varies from $\rho=0$ to $\rho=\rho_{\max}$, where it joins smoothly to the TS_τ variable v_τ at $v_\tau=-1/2\rho_{\max}$. This variable increases through the TS_τ region until its boundary at $v_\tau=0$, where it joins smoothly to S_τ at $S_\tau^{(\min)}$. From here we can easily propagate to the asymptotic value of this variable.

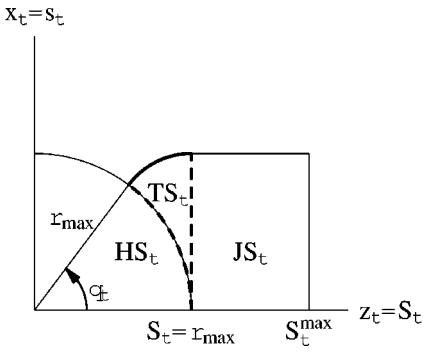

FIG. 10. Hyperspherical (HS_τ), tangent-sphere (TS_τ), and Jacobi (JS_τ) coordinates in the xz plane. The thick dashed curves delimit the TS_τ region. The propagation variable in the HS_τ and JS_τ regions are ρ and S_τ. In the TS_τ region, the propagation variable is v_τ (thick curve).

Use of TS_τ coordinates as an intermediary between the HS_τ system, which is physically appropriate to the situation in which the three particles are in close proximity and strongly interacting, and the JS_τ region, which is appropriate to the asymptotic limit, completely eliminates the need for algebraic or numerical matching procedures such as those described in Sec. II C. Rather, by imposing continuity of the

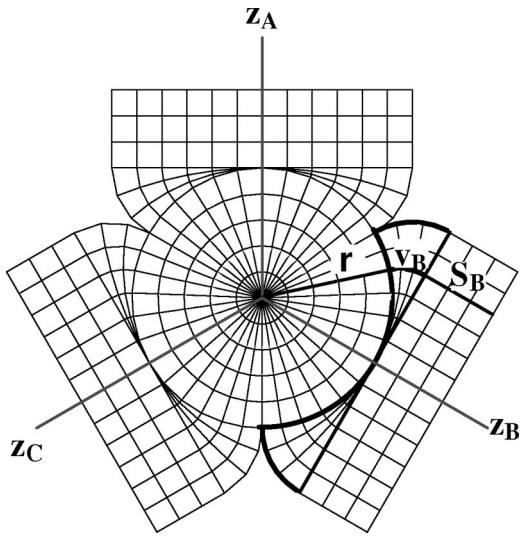

FIG. 11. Bridging the gap between the HS_τ and JS_τ regions (see Fig. 5) with tangent-sphere coordinates. The TS_τ region for $\tau=B$ is delimited by thick curves. After propagating the scattering function in HS_τ coordinates out to $\rho_{\max}$, one transforms this function algebraically to TS_τ coordinates and continues propagating with respect to the variable v_τ. At $v_\tau=0$, one performs a second algebraic transformation to JS_τ coordinates and propagates into the asymptotic region. Note that the arc at $\rho_{\max}$ in the HS_τ region is also the contour of constant $v_\tau=-1/2\rho_{\max}$, and the line of constant S_τ in the JS_τ system is also the contour of constant $v_\tau=0$ in tangent-sphere coordinates.

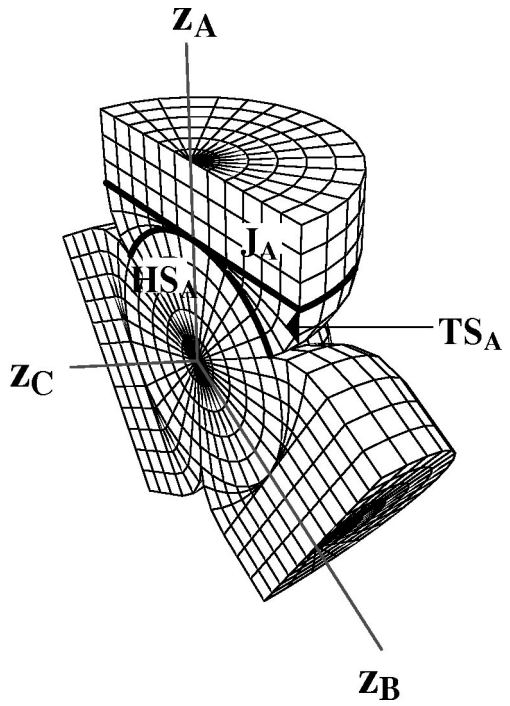

FIG. 12. Jacobi, tangent-sphere, and hyperspherical regions for all arrangement channels of an atom–diatom system with three equal masses. Thick curves highlight the boundaries between the HS_τ and TS_τ region and between the TS_τ and JS_τ regions, both for configuration τ=A. Note that the rotation angle Θ_τ, which is shown in Figs. 3 and 4, is common to all three coordinate systems. The domain of the vibrational coordinate, which is orthogonal to both the rotational and translational coordinate, extends into the classically forbidden (repulsive potential) regions far enough that the vibrational basis functions are essentially zero at the highlighted boundaries.

scattering function and its first derivative at these boundaries we can trivially determine the R matrix at the inner boundary of the TS_τ region from the R matrix at the outer boundary of the HS_τ region (see Sec. II G for details). (In our implementation, a frame transformation is performed at the outer boundary of the HS_τ region to transform to the Delves hyperspherical coordinates.) A similarly simple procedure connects the R matrices at the outer TS_τ boundary and the inner JS_τ boundary. The propagated are lengths given in Table II can be used to ensure that the propagation steps are uniform in each coordinate system.

As noted above, the domains in Eq. (16) are limited in practice by the upper limit $\Theta_\tau=\pi$ and by the proximity of each TS_τ to its adjacent HS_τ and JS_τ regions. For example, the TS_τ translational coordinate v_τ is bounded as indicated in Fig. 10,

$$-\frac{1}{2\rho_{\max}}\leqslant v_\tau\leqslant 0. \tag{18}$$

The JS_τ vibrational coordinate s_τ is bounded at the maximum value $s^{\max}\tau$ by the properties of the vibrational wave functions in the JS_τ basis, which requires that the coordinate w_τ of the TS_τ region be limited to the same physical range. The vibrational coordinate ranges for the TS_τ and JS_τ systems must extend into the classically forbidden region far enough that the basis functions for arrangement τ are essentially zero.

TABLE III. Coordinates and metric coefficients for JS_τ, TS_τ, and HS_τ coordinate systems. The volume elements for the full six-dimensional space is $s_\tau^2 S_\tau^2\sqrt{g}$; see Table II.

	HS_τ	TS_τ	JS_τ	Generalized coordinate
Propagation variable	ρ	v_τ	S_τ	q_1
''Vibrational'' variable	θ_τ	w_τ	s_τ	q_2
g_{11}	1	$\frac{w_\tau^4}{(1+v_\tau^2 w_\tau^2)^2}$	1	
g_{22}	ρ^2	$\frac{1}{(1+v_\tau^2 w_\tau^2)^2}$	1	
$\sqrt{g}$	ρ	$\frac{w_\tau^2}{(1+v_\tau^2 w_\tau^2)^2}$	1	

F. Hamiltonians and expansion bases

The kinetic energy operator in JS_τ coordinates is customarily expressed using spherical coordinates $(S_\tau,\hat{S}_\tau)$, and $(s_\tau,\hat{s}_\tau)$, where $\hat{S}_\tau$ and $\hat{s}_\tau$ denote the polar and azimuthal angles of their respective vectors. Writing the Laplacian operators $\nabla^2_{S_\tau}$ and $\nabla^2_{s_\tau}$ in Eq. (7a) in these coordinates and introducing the orbital angular momentum $\mathbf{L}_\tau$ of atom τ about the center-of-mass of the corresponding diatom, the rotational angular momentum $\mathbf{j}_\tau$ of the diatom, and the total angular momentum $\mathbf{J}=\mathbf{j}_\tau+\mathbf{L}_\tau$, the kinetic energy operator becomes

$$T=-\frac{\hbar^2}{2\mu}\frac{1}{s_\tau S_\tau}\left[\frac{\partial^2}{\partial S_\tau^2}+\frac{\partial^2}{\partial s_\tau^2}+\frac{1}{S_\tau^2}L_\tau^2+\frac{1}{s_\tau^2}j_\tau^2\right]s_\tau S_\tau. \tag{19}$$

The system Hamiltonian in JS_τ coordinates is then

$$\mathscr{H}=T+V(S_\tau,s_\tau,\Theta_\tau). \tag{20}$$

To transform the kinetic energy operator into HS_τ or TS_τ coordinates, we simply apply the chain rule using the appropriate conformal transformation from Table I. Let us denote by q_1 the propagation variable in any of the three systems and by q_2 the vibrational coordinate (see Table III). In terms of these generalized coordinates, we can write a generic form for this operator that pertains to any of the three systems:[23]

$$T=-\frac{\hbar^2}{2\mu}\frac{q_1^\kappa q_2^\eta}{S(q_1,q_2)s(q_1,q_2)}\left[\sum_{i=1}^{2}\frac{1}{\sqrt{g}}\frac{\partial}{\partial q_i}\left(g_{ii}\sqrt{g}\frac{\partial}{\partial q_i}\right)+\frac{L^2}{S^2(q_1,q_2)}+\frac{j^2}{s^2(q_1,q_2)}\right]\frac{S(q_1,q_2)s(q_1,q_2)}{q_1^\kappa q_2^\eta}, \tag{21}$$

where the metric coefficients g_{ii} and $\sqrt{g}$ are given in Table III. The exponents in the factors q_1^κ and q_2^η are chosen to eliminate first derivative terms from the resulting kinetic energy operator in each system; in JS_τ coordinates, for example, $\kappa=\eta=0$, and the kinetic energy operator is (19). The inverses of $q_1^\kappa q_2^\eta$ multiply the corresponding radial functions in Tables IV and V. The kinetic energy operators in the HS_τ system that results from applying Eq. (21) is

TABLE IV. The Schrödinger equations used to define the vibrational functions in the space-fixed and body-fixed bases. In the HS_τ system, different vibrational bases are used in different sectors, as discussed in the text. For clarity, however, we suppress the sector index on ρ.

Region	Vibrational Schrödinger equation
Hyperspherical	$\left\{-\frac{\hbar^2}{2\mu}\frac{1}{\rho^2}\left[\frac{\partial^2}{\partial\theta_\tau^2}+\frac{j_\tau(j_\tau+1)}{\sin^2\theta_\tau}\right]+V_\tau(\rho\sin\theta_\tau)-E_{\nu,j}^{(\mathrm{HS})}(\rho)\right\}\times\phi_{vj}^{(\mathrm{HS})}(\theta_\tau)=0$
Tangent sphere	$\left\{-\frac{\hbar^2}{2\mu}(1+v_\tau^2w_\tau^2)^2\left[\frac{\partial^2}{\partial w_\tau^2}+\frac{j_\tau(j_\tau+1)}{w_\tau^2}\right]+V_\tau\left(\frac{w_\tau}{1+v_\tau^2w_\tau^2}\right)-E_{\nu,j}^{(\mathrm{TS})}(v_\tau)\phi_{vj}^{(\mathrm{TS})}(w_\tau)=0\right.$
Jacobi	$\left\{-\frac{\hbar^2}{2\mu}\left[\frac{\partial^2}{\partial s_\tau^2}+\frac{j_\tau(j_\tau+1)}{s_\tau^2}\right]+V_\tau(s_\tau)-E_{\nu,j}^{(\mathrm{JS})}\right\}\phi_{vj}^{(\mathrm{JS})}(s_\tau)=0$

$$T=-\left(\frac{\hbar^2}{2\mu}\right)\frac{2}{\rho^{5/2}\sin 2\theta_\tau}\left[\frac{\partial^2}{\partial\rho^2}+\frac{1}{\rho^2}\frac{\partial^2}{\partial\theta_\tau^2}+\frac{1}{4\rho^2}+\frac{1}{\rho^2\cos^2\theta_\tau}L_\tau^2+\frac{1}{\rho^2\sin^2\theta_\tau}j_\tau^2\right]\frac{\rho^{5/2}\sin 2\theta_\tau}{2}, \tag{22}$$

and that for the TS_τ system is

$$T=-\left(\frac{\hbar^2}{2\mu}\right)\frac{1}{w_\tau^2}\frac{(1+v_\tau^2w_\tau^2)^2}{v_\tau w_\tau^2+\rho_{\max}(1+v_\tau^2w_\tau^2)}\times\left\{(1+v_\tau^2w_\tau^2)^2\left[\frac{1}{w_\tau^4}\frac{\partial^2}{\partial v_\tau^2}+\frac{\partial^2}{\partial w_\tau^2}\right]+\frac{(1+v_\tau^2w_\tau^2)^2}{[v_\tau w_\tau^2+\rho_{\max}(1+v_\tau^2w_\tau^2)]^2}L_\tau^2+\frac{(1+v_\tau^2w_\tau^2)^2}{w_\tau^2}j_\tau^2\right\}\times w_\tau^2\frac{v_\tau w_\tau^2+\rho_{\max}(1+v_\tau^2w_\tau^2)}{(1+v_\tau^2w_\tau^2)^2}. \tag{23}$$

The exponents in the scale factors for the HS_τ coordinates are $\kappa=1/2$ and $\eta=0$; those for the TS_τ coordinates are $\kappa=0$ and $\eta=1$.

In each coordinate system, we solve the Schrödinger equation for the scattering function by expanding the system wave function in a basis that is complete in the vibrational and angular coordinates of that system. For scattering from an initial channel $\gamma_0=(\tau_0,\nu_0,j_0,l_0;JMp)$, we denote the wave function by $\Psi_{\gamma_0}(\mathbf{q}_1,\mathbf{q}_2)$, leaving implicit the constants of the motion J, M, and the parity

$$p=(-1)^{j+l}. \tag{24}$$

All channel indices contain J, M, p, and the arrangement channel index τ. In addition, space-fixed channels are distinguished by the quantum numbers v, j, and l, corresponding to the vibrational Hamiltonian, $\mathbf{j}_\tau$, and $\mathbf{L}_\tau$, respectively. To specify channels the body frame, we replace l by the Λ, which corresponds to projection of $\mathbf{L}_\tau$ on the body-frame z_τ axis. Thus in the body frame, the initial channel is $\gamma_0=(\tau_0,\nu_0,j_0,\Lambda_0;JMp)$.[20,7] The general form of the expansion, for any coordinate system in either body-fixed or space-fixed reference frames, is

$$\Psi_{\gamma_0}(\mathbf{q}_1,\mathbf{q}_2)=\sum_\gamma G_{\gamma,\gamma_0}(q_1)\Phi_\gamma(\hat{\mathbf{q}}_1,\mathbf{q}_2), \tag{25}$$

where $\{\Phi_\gamma(\hat{\mathbf{q}}_1,\mathbf{q}_2)\}$ is the appropriate basis.

In each coordinate system, the functions in this basis are products of vibrational wave functions for the diatom and angular functions for either the body- or space-fixed frames. In the body-fixed JS_τ system, for example, the basis consists of products of functions $\phi_{vj}^{(\mathrm{JS})}(s_\tau)$ and associated Legendre polynomials $P_j^\Lambda(\cos\Theta_\tau)$, which represent rotational eigenstates of the diatom. The JS_τ vibrational Hamiltonian whose eigenfunctions appear in this basis is given in Table IV, along with those for the HS_τ and TS_τ systems.

In the expansion of $\Psi_{\gamma_0}(\mathbf{q}_1,\mathbf{q}_2)$ in this basis, the body-fixed JS_τ radial function $G_{\gamma,\gamma_0}^{(\mathrm{JS})}(S_\tau)$ is multiplied by the scale factor $1/s_\tau S_\tau$ to cancel the factor $q_1q_2=s_\tau S_\tau$ in the JS_τ kinetic energy operator (19). Finally, the expansion is multiplied by the normalized Wigner rotation matrix[17] to take account of the overall orientation of the system. There results the JS_τ expansion of the body-fixed wave function,

$$\Psi_{\gamma_0}(\mathbf{q}_1,\mathbf{q}_2)=\sum_{\gamma'}\mathcal{D}_{\Lambda',M}^J(\alpha_{\tau'},\beta_{\tau'},\gamma_{\tau'})\frac{1}{S_{\tau'}s_{\tau'}}\times G_{\gamma',\gamma_0}^{(\mathrm{JS})}(S_{\tau'})\phi_{v'j'}^{(\mathrm{JS})}(s_{\tau'})P_{j'}^{\Lambda'}(\cos\Theta_{\tau'}). \tag{26a}$$

The Wigner rotation matrix effects rotation into the space fixed frame and so is not required for the corresponding space-fixed expansion. Rather, the rotational functions $P_j^\Lambda(\cos\Theta_\tau)$ are replaced by coupled angular functions that take into account rotations of the diatom and its orientation in the space-fixed frame,

$$\mathcal{Y}_{jl}^{JM}(\hat{S}_\tau,\hat{s}_\tau)=\sum_{\Lambda',m'}C(j'l'J;\Lambda'm'M)Y_{j',\Lambda'}(\hat{s}_\tau)Y_{l',m'}(\hat{S}_\tau), \tag{26b}$$

where we adopt the conventions of Rose for the Clebsch–Gordan coefficients.[17] The expansion of the space-fixed wave function in the JS_τ basis is

TABLE V. Space-fixed expansion of the system wave function $\Psi_{\gamma_0}(\mathbf{q}_1,\mathbf{q}_2)$ for HS_τ, TS_τ, and JS_τ coordinate systems. The channel indices for these expansions are $\gamma=(\tau,\nu,j,l;JMp)$. The subscript 0 denotes the initial channel.

Region	Space-fixed expansion
Hyperspherical	$\sum_{\gamma'}\frac{2}{\rho^{5/2}\sin 2\theta_{\gamma'}}G_{\gamma',\gamma_0}^{(\mathrm{HS})}(\rho)\phi_{v'j'}^{(\mathrm{HS})}(\theta_{\gamma'})\mathcal{Y}_{j'l'}^{JM}(\hat{S}_{\tau'},\hat{s}_{\tau'})$
Tangent sphere	$\sum_{\gamma'}\frac{(1+v_{\gamma'}^2w_{\gamma'}^2)^2}{w_{\gamma'}^2(v_{\gamma'}w_{\gamma'}^2+\rho_{\max}+v_{\gamma'}^2w_{\gamma'}^2\rho_{\max})}G_{\tau',\gamma_0}^{(\mathrm{TS})}(v_{\gamma'})\times\phi_{v'j'}^{(\mathrm{TS})}(w_{\tau'})\mathcal{Y}_{j'l'}^{JM}(\hat{S}_{\tau'},\hat{s}_{\tau'})$
Jacobi	$\sum_{\gamma'}\frac{1}{S_{\tau'}s_{\tau'}}G_{\gamma',\gamma_0}^{(\mathrm{JS})}(S_{\tau'})\phi_{v'j'}^{(\mathrm{JS})}(s_{\tau'})\mathcal{Y}_{j'l'}^{JM}(\hat{S}_{\tau'},\hat{s}_{\tau'})$

TABLE VI. Body-fixed expansion of the system wave function $\Psi_{\gamma_0}(\mathbf{q}_1,\mathbf{q}_2)$ for HS_τ, TS_τ, and JS_τ coordinate systems. The channel indices for these expansions are $\gamma=(\tau,\nu,j,\Lambda;JMp)$. The subscript 0 denotes the initial channel.

Region	Body-fixed expansion
Hyperspherical	$\sum_{\gamma'} \frac{2}{\rho^{5/2}\sin 2\theta_{\tau'}} G^{(\mathrm{HS})}_{\gamma',\gamma 0}(\rho)\phi^{(\mathrm{HS})}_{v'j'}(\theta_{\tau'}) \times P^{\Lambda'}_{j'}(\cos\Theta_{\tau'})\mathcal{D}^{J}_{\Lambda',M}(\alpha_{\tau'},\beta_{\tau'},\gamma_{\tau'})$
Tangent sphere	$\sum_{\gamma'} \frac{(1+\nu^2_{\tau'}w^2_{\tau'})^2}{w^2_{\tau'}(\upsilon_{\tau'}w^2_{\tau'}+\rho_{\max}+\upsilon^2_{\tau'}w^2_{\tau'}\rho_{\max})} G^{(\mathrm{TS})}_{\gamma',\gamma_0}(\upsilon_{\tau'}) \times \phi^{(\mathrm{TS})}_{v'j'}(w_{\tau'})P^{\Lambda'}_{j'}(\cos\Theta_{\tau'})\mathcal{D}^{J}_{\Lambda',M}(\alpha_{\tau'},\beta_{\tau'},\gamma_{\tau'})$
Jacobi	$\sum_{\gamma'} \frac{1}{S_{\tau'}s_{\tau'}} G^{(\mathrm{JS})}_{\gamma',\gamma_0}(S_{\tau'})\phi^{(\mathrm{JS})}_{v'j'}(s_{\tau'}) \times P^{\Lambda'}_{j'}(\cos\Theta_{\tau'})\mathcal{D}^{J}_{\Lambda',M}(\alpha_{\tau'},\beta_{\tau'},\gamma_{\tau'})$

$$\Psi_{\gamma_0}(\mathbf{q}_1,\mathbf{q}_2)=\sum_{\gamma'}\frac{1}{S_{\tau'}s_{\tau'}}G^{(\mathrm{JS})}_{\gamma',\gamma_0}(S_{\tau'}) \times\phi^{(\mathrm{JS})}_{v'j'}(s_{\tau'})\mathcal{Y}^{JM}_{j'l'}(\hat{S}_{\tau'},\hat{s}_{\tau'}). \tag{26c}$$

Corresponding expansions of $\Psi_{\gamma_0}(\mathbf{q}_1,\mathbf{q}_2)$ in HS_τ and TS_τ systems are given in Table V for the space-fixed frame and Table VI for the body-fixed frame. In regard to the TS_τ basis, note that the TS_τ vibrational Hamiltonian in Table IV depends on the TS_τ translational coordinate υ_τ in addition to the vibrational coordinate w_τ. Hence the TS_τ vibrational wave functions depend parametrically on υ_τ. In practice, this features causes no problems. The set $\{\phi^{(\mathrm{TS})}_{vj}(w_\tau)\}$ is complete for any υ_τ in the physically relevant range $-1/2\rho_{\max}\leqslant\upsilon_\tau\leqslant 0$. For example, by choosing $\upsilon_\tau=0$ in this Hamiltonian, we can make the vibrational Hamiltonians (and wave functions) in the JS_τ and TS_τ systems identical.

G. Transforming the scattering function at boundaries between coordinate systems

As discussed in Sec. II E, the use of tangent sphere coordinates greatly facilitates propagation of the scattering function from the origin to the asymptotic region because it replaces computationally intensive matching procedures (at values of the propagation variable where a change of coordinate system is made) by simple matrix transformations. At either the HS_τ–TS_τ boundary or at the TS_τ–JS_τ boundary, we merely impose continuity of the scattering function $\Psi_{\gamma_0}(\mathbf{q}_1,\mathbf{q}_2)$ and its first derivative with respect to the propagation coordinate q_1. This chore is made easier by introducing the R matrix, which is defined (in any coordinate system) by the matrix product

$$\mathbf{R}(q_1)=\mathbf{G}(q_1)[\mathbf{G}'(q_1)]^{-1}. \tag{27}$$

Each boundary defines two regions: the one to its left and the one to its right. The continuity conditions concern the propagation variable as it changes between these regions. We denote this variable in the left region by q_1 and in the right region by $\overline{q_1}$. At the HS_τ–TS_τ boundary, for example, the maximum propagation coordinate for the left region, $q_1^{\max}$, is $\rho_{\max}$, while the minimum coordinate for the right region, $\overline{q}_1^{\max}$, is $\upsilon_\tau^{(\min)}$. Propagation and vibrational coordinates at both boundaries appear in Table VII.

TABLE VII. Values of the propagation and vibrational coordinates at the boundaries between the HS_τ, TS_τ, and JS_τ regions. The third column gives relationships between the vibrational coordinates q_2 in each region for values of q_1 given in the second column.

Coordinate system	propagation coordinate (q_1)	vibrational coordinate (q_2)
	HS_τ–TS_τ boundary	
HS_τ	$\overline{q}_1^{\max}=\rho_{\max}$	$\theta_\tau=2\tan^{-1}\left(\frac{w_\tau}{2\rho_{\max}}\right)$
TS_τ	$q_1^{\min}=\upsilon_\tau^{(\min)}=-\frac{1}{2\rho_{\max}}$	$w_\tau=2\rho_{\max}\tan\left(\frac{\theta_\tau}{2}\right)$
	TS_τ–JS_τ boundary	
TS_τ	$\upsilon_\tau^{(\max)}=0$	$w_\tau=s_\tau$
JS_τ	$S_\tau^{(\min)}=\rho_{\max}$	$s_\tau=w_\tau$

Imposing continuity of the scattering function at either boundary yields

$$\Psi_{\gamma_0}(\mathbf{q}_1,\mathbf{q}_2)|_{q_1=q_1^{\max}}=\Psi_{\gamma_0}(\overline{\mathbf{q}}_1,\overline{\mathbf{q}}_2)|_{\overline{q}_1=\overline{q}_1^{\min}}. \tag{28a}$$

Inserting the generic expansion (25) and using orthogonality of the basis functions appropriate to the left region, $\Phi_\gamma(\hat{\mathbf{q}}_1,\mathbf{q}_2)$, yields

$$G_{\gamma,\gamma_0}(q_1^{\max})=\sum_{\gamma'}\overline{G}_{\gamma',\gamma_0}(\overline{q}_1^{\min})\langle\Phi_\gamma|\overline{\Phi}_{\gamma'}\rangle_{q_1=q_1^{\max}}. \tag{28b}$$

We can write this result in matrix notation as

$$\mathbf{G}(q_1^{\max})=\mathbf{O}\overline{\mathbf{G}}(\overline{q}_1^{\min}), \tag{28c}$$

where $\mathbf{O}$ is the matrix whose elements are overlap integrals between expansion bases for the adjacent regions.

Similarly, imposing continuity of the scattering function at a boundary yields

$$\frac{\partial}{\partial q_1}\Psi_{\gamma_0}(\mathbf{q}_1,\mathbf{q}_2)\bigg|_{q_1=q_1^{\max}}=\frac{\partial}{\partial q_1}\Psi_{\gamma_0}(\overline{\mathbf{q}}_1,\overline{\mathbf{q}}_2)\bigg|_{\overline{q}_1=\overline{q}_1^{\min}}, \tag{29a}$$

$$=\frac{\partial\overline{q}_1}{\partial q_1}\frac{\partial}{\partial\overline{q}_1}\Psi_{\gamma_0}(\mathbf{q}_1,\mathbf{q}_2)\bigg|_{q_1=\overline{q}_1^{\min}}. \tag{29b}$$

Note that $\partial\overline{q}_2/\partial q_1$ is zero at any region boundary, because at a boundary unit vectors along $\overline{\mathbf{q}}_1$ and $\mathbf{q}_1$ are parallel. The quantity $\partial\overline{q}_1/\partial q_1$ in (29b) is just the scale factor for the transformation $(\overline{\mathbf{q}}_1,\overline{\mathbf{q}}_2)\rightarrow(\mathbf{q}_1,\mathbf{q}_2)$. Application of the generic expansion of $\Psi_{\gamma_0}(\mathbf{q}_1,\mathbf{q}_2)$ and orthogonality of basis functions for the left region yields a matrix equation for the first derivatives that is analogous to Eq. (28c),

$$\mathbf{G}'(q_1^{\max})=\mathbf{Q}\overline{\mathbf{G}}'(\overline{q}_1^{\min}), \tag{30}$$

where $\mathbf{Q}$ is the matrix of scale factors at the boundary.

Combining Eqs. (28c) and (30), we obtain the desired transformation equation for the R matrix at a region boundary,

$$\mathbf{R}(q_1^{\max})=\mathbf{O}\overline{\mathbf{R}}(\overline{q}_1^{\min})[\mathbf{Q}]^{-1}. \tag{31}$$

To complete this description we need only determine the scale factors at each of the region boundaries. We can facilitate implementation of Eq. (31) by judiciously exploiting the aforementioned parametric dependence of the TS_τ vibrational Hamiltonian on v_τ. If we choose $v_\tau=-1/2\rho_{\max}$ in this Hamiltonian, then the basis functions in the HS_τ and TS_τ regions are identical. The overlap matrix **O** in (31) then reduces to the identity matrix. Moreover, since at this boundary $\partial\overline{q_1}/\partial q_1=w_\tau^{-2}$, the elements of the matrix **Q** of scale factors are simply

$$\left\langle \Phi_\gamma \left| \frac{1}{w_\tau^2} \right| \overline{\Phi}_{\gamma'} \right\rangle_{q_1=q_1^{\max}} = \int \phi_{vj}^{(\mathrm{HS})}(\theta_\tau)\frac{1}{w_\tau^2}\phi_{v'j'}^{(\mathrm{TS})}(w_{\tau'})dw_{\tau'}. \tag{32}$$

Note that for this choice of v_τ, the vibrational coordinates w_τ and θ_τ are related by

$$w_\tau=2\rho_{\max}\tan\left(\frac{\theta_\tau}{2}\right), \tag{33}$$

so we can evaluate the one-dimensional integral in (32) with respect to either w_τ or θ_τ.

At the TS_τ–JS_τ boundary, we choose $v_\tau=0$ in the TS_τ vibrational Hamiltonian. This choice makes the TS_τ and JS_τ vibrational basis functions identical, and again reduces the overlap matrix **O** in Eq. (31) to the unit matrix. The scale factor at this boundary is again equal to w_τ^{-2}, so the matrix elements of **Q** have the same form as those in Eq. (32). Since at $v_\tau=0$, the TS_τ and JS_τ vibrational coordinates are equal, $w_\tau=s_\tau$, we can easily evaluate these matrix elements in the JS_τ system.

H. Calculating the differential cross section from the *R* matrix

Once the propagation described in the previous section has reached the asymptotic region, a value $S_\tau^{(\max)}$ in the JS_τ coordinate system, we extract the *K* matrix, with elements $K_{\gamma,\gamma'}$, by matching the JS_τ scattering function to the usual asymptotic boundary conditions,

$$G_{\gamma,\gamma_0}^{(\mathrm{JS})}(S_\tau)=\mathbf{a}(S_\tau)-\mathbf{b}(S_\tau)\mathbf{K}. \tag{34}$$

For open channels, the elements of **a** and **b** are proportional to the Ricatti–Bessel and Neumann functions, respectively,[24]

$$a_{\gamma,\gamma_0}=\delta_{\gamma,\gamma_0}k_\gamma^{1/2}S_\tau\hat{j}_l(k_\gamma S_\tau), \tag{35a}$$

$$b_{\gamma,\gamma_0}=\delta_{\gamma,\gamma_0}k_\gamma^{1/2}S_\tau\hat{n}_l(k_\gamma S_\tau), \tag{35b}$$

where the channel wavenumber k_γ is defined by conservation of the total system energy *E* in terms of the rovibrational energies $\epsilon_{v,j}$ of the diatom as

$$E=\frac{\hbar^2}{2\mu}k_0^2+\epsilon_{v_0,j_0}=\frac{\hbar^2}{2\mu}k_\gamma^2+\epsilon_{v,j}. \tag{36}$$

For asymptotically closed channels, the matching conditions are

$$G_{\gamma,\gamma_0}^{(\mathrm{JS})}(S_\tau)=\mathbf{c}(S_\tau)-\mathbf{d}(S_\tau)\mathbf{K}. \tag{37}$$

Defining

$$k_\gamma=i\kappa_\gamma, \tag{38}$$

where $\kappa_\gamma=|k_\gamma|$, we follow McLenithan and Secrest[25] in choosing

$$c_{\gamma,\gamma_0}=\delta_{\gamma,\gamma_0}\kappa_\gamma^{1/2}S_\tau\hat{j}_l(i\kappa_\gamma S_\tau), \tag{39a}$$

$$d_{\gamma,\gamma_0}=\delta_{\gamma,\gamma_0}\kappa_\gamma^{1/2}S_\tau\hat{h}_l^{(1)}(i\kappa_\gamma S_\tau). \tag{39b}$$

The quantities a_{γ,γ_0} are real and closely related to the modified spherical Bessel functions $I_{l_\gamma+1/2}$, which are regular at the origin. The quantities b_{γ,γ_0} are also real. They are closely related to the modified spherical Bessel functions $K_{l_\gamma+1/2}$, which decay to zero exponentially at large distances.[24]

With these conventions, we can determine the *K* matrix from the *R* matrix (27) at S_τ as

$$\mathbf{K}=(\mathbf{R}\mathbf{b}'-\mathbf{b})^{-1}(\mathbf{R}\mathbf{a}'-\mathbf{a}), \tag{40}$$

where $\mathbf{a}'$ and $\mathbf{b}'$ are the first derivatives of **a** and **b** evaluated at S_τ.

If the boundary conditions given above are applied before the dying closed-channel coefficients d_{γ,γ_0} are negligible, then the resulting *K* matrix will contain elements corresponding to both open and closed channels. The cross section, however, depends only on the scattering matrix between open channels. So only the open–open block $\mathbf{K}_{oo}$ of the full *K* matrix contributes to the *S* matrix,[25]

$$\mathbf{S}=(\mathbf{I}+i\mathbf{K}_{oo})(\mathbf{I}-i\mathbf{K}_{oo})^{-1}. \tag{41}$$

From the *S* matrix, we calculate the transition matrix, with the convention $\mathbf{T}=\mathbf{I}-\mathbf{S}$, and thence the scattering amplitude for a transition (in the space-fixed frame),

$$\gamma_0=(\tau_0,\nu_0,j_0,l_0;JMp)\rightarrow\gamma=(\tau,\nu,j,l;JMp). \tag{42}$$

In terms of elements of **T**, this amplitude is

$$f(\mathbf{k}_\gamma,\gamma\leftarrow\mathbf{k}_0,\gamma_0)=\frac{2\pi}{\sqrt{k_\gamma k_0}}\sum_{JM}\sum_{ll_0}i^{l_0-l+1}\times C(jlJ;m,M-m,M)Y_{l,M-m_0}^*(\hat{\mathbf{k}}_0)\times Y_{l,M-m}(\hat{\mathbf{k}}_\gamma)T_{\gamma,\gamma_0}^J, \tag{43}$$

where $\hat{\mathbf{k}}_\gamma=\hat{S}_\tau$ denotes the scattering angle in the final state. Finally, the differential cross section for this transition is

$$I_{\gamma_0\rightarrow\gamma}(\hat{S}_\tau)=\frac{k_\gamma}{k_0}|f(\mathbf{k}_\gamma,\gamma\leftarrow\mathbf{k}_0,\gamma_0)|^2. \tag{44}$$

III. IMPLEMENTATION

To summarize the tangent sphere procedure and as a guide to future applications, here we outline the implementation for reactive collisions of the type shown in Eq. (1a). Figure 12 combines all three regions and shows the demarcation boundaries referred to in this description.

(1) Choose the range of total energies *E* over which we require cross sections for comparison to experiment.

(2) Estimate the number of required vibrational basis functions and calculate vibrational wave functions for each arrangement channel in the asymptotic limit using analytic basis sets consisting of Sturmian functions for Coulombic systems or simple harmonic oscillator eigenfunctions for molecular systems. Integrals are evaluated using Gauss–Hermite quadrature designed to conform to the maximum value of s_τ as determined by the extent of the vibrational basis functions.

(3) Calculate the maximum propagation radius in the HS_τ region, $\rho_{\max,}$ from Eqs. (14). Using vibrational wave functions $\phi_{vj}^{(HS)}(\theta_\tau)$ at $\rho_{\max}$, we check convergence of the vibrational eigenenergies with respect to the number of basis functions, increasing the number of these functions if necessary. These tests ensure that our basis is adequate in hyperspherical coordinates at $\rho_{\max}$ and in Jacobi coordinates for $\rho_{\max} \leqslant S_\tau \leqslant \infty$. Since this basis is also adequate at the HS_τ–TS_τ and HS_τ–JS_τ boundaries, it is comparably accurate over the entire TS_τ region, $-1/2\rho_{\max} \leqslant v_\tau \leqslant 0$.

(4) Generate contour plots of the interaction potential in hyperspherical coordinates at several values of the hyperradius. From these we estimate the initial value of ρ for the propagation, making sure that all contours at that value of ρ are much higher than the maximum energy at which we will calculate cross sections. This check ensures that for all energies propagation will begin in the classically forbidden region.

(5) Calculate HS_τ surface functions and eigenenergies at several values of ρ near $\rho_{\max}$, using the discrete variable representation, analytic basis set method, or finite element method. Using these we make the estimated starting value of ρ precise via the WKB approximation. We are quite conservative in our choice of this minimum value of ρ.

(6) Generate surface functions and coupled equations in the HS_τ region, storing on disk matrix elements and overlaps to be used in the transformations from one sector to another discussed in Sec. II C. This fairly extensive calculation requires numerous convergence checks and substantial disk space. This step, however, is the last one before propagation.

(7) Propagate the R matrix in hyperspherical coordinates from our initial value of ρ to $\rho_{\max}$, where we switch from APH coordinates to Delves coordinates. We then transform the R matrix function to TS_τ coordinates using Eq. (31) with the simplifications discussions in Sec. II G. This initializes the propagation with respect to v_τ through the TS_τ region. At the outer boundary of this region, we again implement the equations of Sec. II G to transform the T matrix into the JS_τ region. Further propagation with respect to S_τ yields the scattering function at a value of this coordinate large enough that the matching equations of Sec. II H are applicable. This yields the K matrix, from which we calculate the desired cross sections.

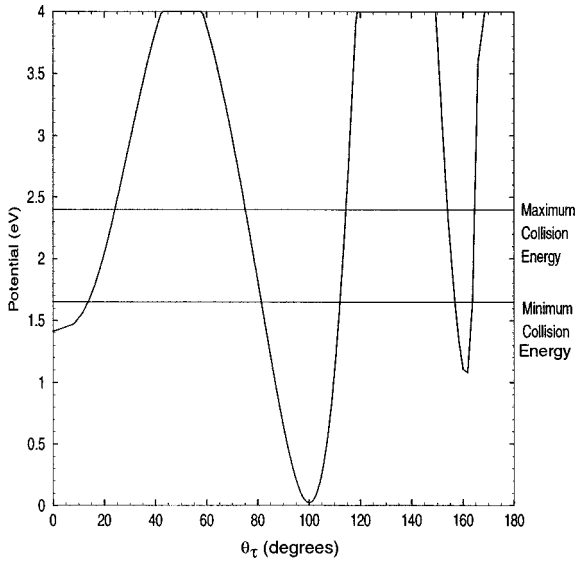

FIG. 13. Colinear barrier heights for rearrangement processes illustrated by a two-dimensional ''slice'' through the T5a potential surface $V(\rho = 6.975, \theta_{\mathrm{APH}} = \pi/2, \chi_{\mathrm{APH}})$ of Brown *et al.* in APH coordinates at a hyperradius of $\rho_{\max} = 6.975 a_0$.

IV. APPLICATION TO F+H_2 SCATTERING

Since the $F + H_2 \rightleftharpoons HF + F$ reaction continues to be the focus of both theoretical and experimental activity we choose this system to demonstrate the effectiveness of the tangent sphere method. In this section we compare results calculated with the tangent sphere against those from previous calculations in which we used a two-dimensional projection of asymptotic Jacobi solutions onto a hypersphere of radius[26–28] $\rho_{\mathrm{asym}} = 9.5 a_0$. In both calculations we used the potential energy surface of Brown *et al.* (often referred to as the T5a or Truhlar 5a potential)[29] (see Fig. 13).

In this reaction two of the particles are identical, and we identify arrangement channels as A=F and B=C=H. We performed scattering calculations at 95 values of the total energy in the range $1.65\,\mathrm{eV} \leqslant E \leqslant 2.4\,\mathrm{eV}$. Figure 14 shows colinear contours for this system. The dashed contour corresponds to the maximum collision energy, 2.4 eV. As this diagram shows, $\rho_{\max}$ must be greater than $\approx 6.8 a_0$ to allow for tunneling in the interior hyperspherical region. We evaluated the values of $s^{\max}$, the largest Gauss–Hermite quadrature point for each arrangement channel, using the same vibrational basis and parameters as in our previous calculations;[26–28] these values are given in Table VIII. The skew angles and scale factors in this table were calculated from the atomic masses. Using Eq. (14) we obtained $\rho_{\max} = 6.83_0$. So we could use surface functions from our previous calculations[26–28] in propagation through the hyperspherical region, we choose $\rho_{\max} = 6.975 a_0$, a value at which a previously calculated surface function was available.[26–28] Figure 15 shows hyperspherical (APH) contours for a constant hyperradius of $6.875 a_0$. Figure 13 shows that for this value of $\rho_{\max}$ the barrier height for scattering from channel A to channels B or C is 3.9 eV with a width of $1.6 a_0$ at the maximum collision energy, and the barrier height from channel B to C is 710 eV with a width of $5.4 a_0$ at the maximum

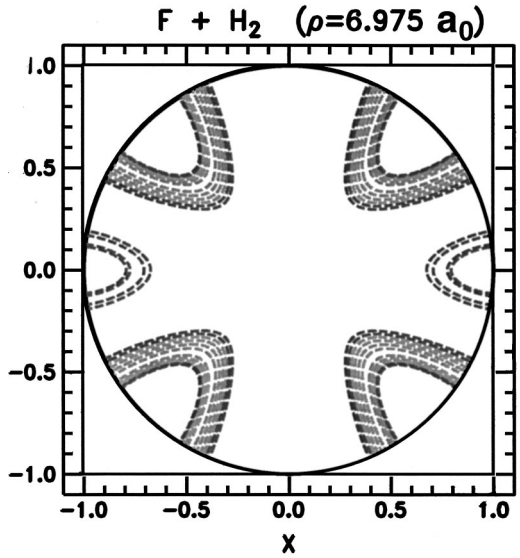

FIG. 14. Potential energy contour plot of the T5a potential energy surface of Brown *et al.* in APH coordinates at a hyperradius of $\rho_{\max}=6.975a_0$. The white areas are classically forbidden regions where the potential energy is greater than the maximum collision energy of 2.4 eV (solid circle).

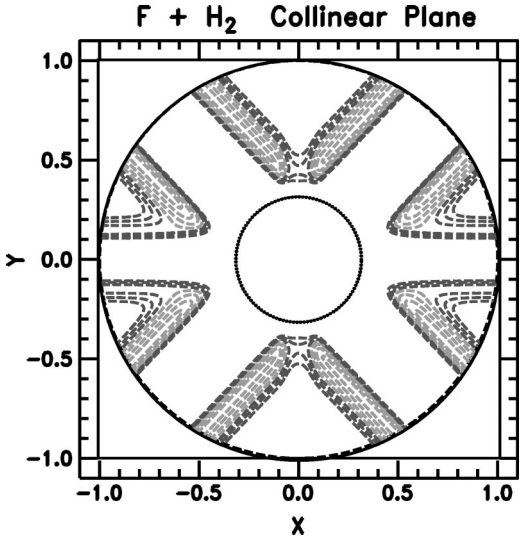

FIG. 15. Potential energy contour plot of the T5a potential energy surface of Brown *et al.*[29] for the colinear configuration. The white areas are classically forbidden regions where the potential energy is greater than the maximum collision energy of 2.4 eV. The outer circle is the hyperradius ρ_{asym} of our previous calculations.[26–28] The inner circle is the hyperradius $\rho_{\max}$ for current implementation of the tangent-sphere technique.

collision energy. These values ensure that tunneling in the tangent-sphere and Jacobi regions is negligible at all scattering energies of interest.

We propagated the coupled-channel equations from $\rho=2.2a_0$ to $\rho=\rho_{\max}$ in the hyperspherical region using APH coordinates. We then applied the unitary transformation to transform the R matrix from APH to Devles coordinates. Using Eq. (31) to evaluate the R matrix in the tangent-sphere region, we then propagated through that region. Finally we again used Eq. (31) to evaluate the R matrix in the Jacobi region, after which we propagated through that region from $S_\tau=\rho_{\max}$ to $20a_0$, at which we applied asymptotic boundary conditions.

Figure 16 shows reaction probability $P^R_{\nu_f\leftarrow(\nu_i,j_i)}(E)$ for scattering from initial state $(\nu_i,j_i)=(0,0)$ into a final vibrational manifold ν_f (summed over all final open rotational states) as a function of the total energy E(eV) for the $F+H_2$ system with total angular momentum $J=0$. The curves correspond to the present tangent sphere calculations and the dots to our previous results.[26–28] Clearly, results from the two calculations are identical to graphical accuracy. Since the size of the hyperspherical region in the present calculations is roughly half that in our previous study,[26–28] the present calculations require roughly a factor of 2 less computation time. More importantly, the current procedure completely eliminates the matching procedure required in other methods.

TABLE VIII. Parameters used in the present tangent-sphere calculations and in a benchmark calculations based on a two-dimensional projection of asymptotic Jacobi solutions onto a hypersphere of radius $\rho_{\text{asym}}=9.5a_0$.

Parameter	Channel A	Channel B or C
Atomic mass (amu)	18.9984032	1.00782503
d_τ	1.379	1.00
$\chi_{\tau,\tau'}$	2.3309960	1.6211932
w_e (a.u.)	2.00534×10^{-2}	1.885557×10^{-2}
r_e (a_0)	1.40112	1.732517
$\nu_{\max}$	1	1
$j_{\max}$	12	31
$s^{\max}(a_0)$	2.770	3.352
$\rho_{\max}=S_{\min}(a_0)$	6.975	6.975
$S^{\max}(a_0)$	20	20

V. CONCLUSIONS

The tangent-sphere method eliminates the need for complicated matching procedures such as those in hyperspherical methods for treating exchange or rearrangement processes. To accomplish this, we use tangent-sphere coordinates to smoothly propagate from hyperspherical coordinates to Jacobi coordinates. The relationships between these coordinates are shown in Figs. 11 and 12 and collected in Table I. For convenience we have gathered most of the key equations required to implement this approach in tables: the scattering equations in Table IV, expansion bases in Tables VI and V and boundary values of the propagation variable and vibrational coordinate in Table VII. We hope that these tables along with the step-by-step implementation scheme in Sec. III will facilitate other applications of tangent-sphere coordinates.

In addition to eliminating the need for numerical matching between the hyperspherical and Jacobi regions, the approach described herein reduces the maximum distance to which one must propagate in hyperspherical coordinates, which is now limited to the range of hyperradii over which rearrangement and/or exchange processes occur. Outside this rearrangement region we use simple Jacobi coordinates to propagate to a sufficiently large distance that all coupling and phase contributions are negligible. In addition to increas-

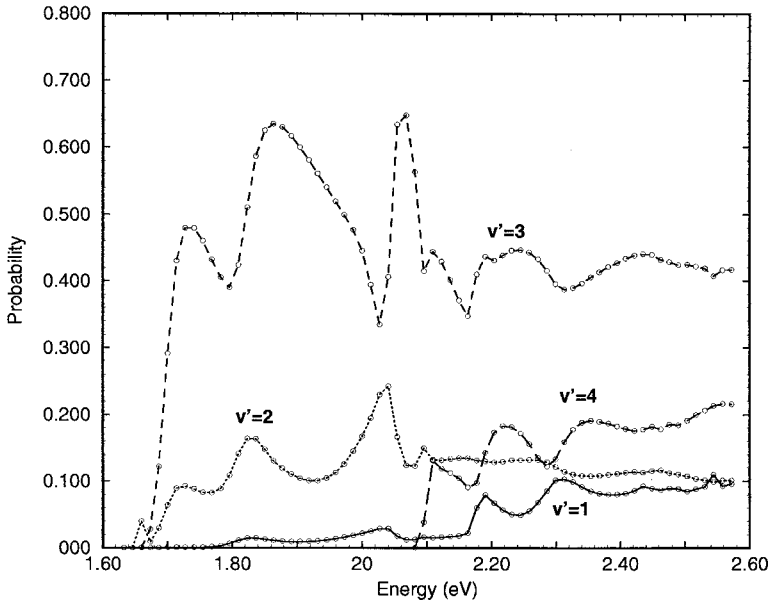

FIG. 16. A comparison of $F+H_2 \rightleftharpoons HF+F$ transition probabilities from our previous calculations[26–28] (solid dots), which uses the two dimension projection technique, with results from the current tangent-sphere procedure (curves).

ing significantly the efficiency of hyperspherical methods, computer programs required by the tangent sphere method are simpler and easier to use.

ACKNOWLEDGMENTS

We acknowledge the support of the National Science Foundation under Grants No. PHY-9722055 and No. CHE-9710383.

[1] N. Barnea, Phys. Rev. A **59**, 1135–1146 (1999).
[2] N. Barnea, W. Leidemann, and G. Orlandini, Nucl. Phys. A **650**, 427 (1999).
[3] B. D. Esry, C. H. Greene, and J. P. Burke, Jr., Phys. Rev. Lett. **83**, 1751 (1999).
[4] B. D. Esry, C. D. Lin, and C. H. Greene, Phys. Rev. A **54**, 394–401 (1996).
[5] D. I. Abramov, L. N. Bogdanova, V. V. Gusev, and L. I. Ponomarev, Phys. At. Nucl. **61**, 457–470 (1998).
[6] A. Kuppermann and G. C. Schatz, J. Chem. Phys. **62**, 2502 (1975); G. C. Schatz and A. Kuppermann, *ibid.* **65**, 4642,4668 (1976).
[7] R. T. Pack and G. A. Parker, J. Chem. Phys. **87**, 3888 (1987) and **90**, 3511 (1989), and references therein.
[8] A. Kuppermann, in *Advances in Molecular Vibrations and Collision Dynamics*, edited by J. Bowman (JAI, Greenwich, CT, 1994), Vol. 2B, pp. 117–186.
[9] A. Kuppermann, J. Phys. Chem. **100**, 2621 (1996).
[10] J. Weiner, V. S. Bagnato, S. Zilio, and P. S. Julienne, Rev. Mod. Phys. **71**, 1 (1999); see especially Chap. VIII.
[11] R. T Pack, E. A. Butcher, and G. A. Parker, J. Chem. Phys. **102**, 5998 (1995); V. J. Barclay, C. E. Dateo, I. P. Hamilton, B. Kendrick, R. T. Pack, and D. W. Schwenke, *ibid.* **103**, 3864 (1995) (communication); B. K. Kendrick, Phys. Rev. Lett. **79**, 2431 (1997); B. K. Kendrick, R. T Pack, R. B. Walker, and E. F. Hayes, J. Chem. Phys. **110**, 6673 (1999).
[12] C. D. Lin, Phys. Rep. **257**, 1 (1995), and references therein.
[13] J. Beradkar and S. Mazevet, J. Phys. B **32**, 3965 (1999); S. Mazevet, I. E. McCarthy, and E. Weigold, Phys. Rev. A **57**, 1881 (1998); S. Mazevet, I. E. McCarthy, D. Madison, and E. Weigold, J. Phys. B **31**, 2187 (1998).
[14] F. T. Smith, J. Chem. Phys. **31**, 132 (1959); Phys. Rev. **120**, 1058 (1960).
[15] L. M. Delves, Nucl. Phys. **9**, 391 (1959); **20**, 275 (1960).
[16] F. T. Smith, J. Math. Phys. **3**, 735 (1962); R. C. Whittenand and R. T. Smith, *ibid.* **9**, 1103 (1968); R. C. Whitten, *ibid.* **10**, 1631 (1969).
[17] M. E. Rose, *Elementary Theory of Angular Momentum* (Wiley, New York, 1957).
[18] L. D. Faddeev, *Mathematical Aspects of the Three-Body Problem in Quantum Scattering Theory* (D. Davey & Co., New York, 1965).
[19] D. A. Micha, J. Chem. Phys. **57**, 2184–2192 (1972).
[20] A. M. Arthurs and A. Dalgarno, Proc. R. Soc. London, Ser. A **256**, 540 (1960).
[21] O. I. Tolstikhin, S. Watanabe, and M. Matsuzawa, J. Phys. B **29**, L389 (1996).
[22] Y. Sun, D. J. Kouri, and D. G. Truhlar, Nucl. Phys. A **508**, 41c–62c (1990).
[23] P. Moon and D. E. Spencer, *Field Theory Handbook, Including Coordinate Systems, Differential Equations and Their Solutions* (Springer-Verlag, Berlin, 1971).
[24] M. Abramowitz and I. A. Stegun, in *Handbook of Mathematical Functions* (Dover, New York, 1968).
[25] K. D. McLenithan, Ph.D. thesis, University of Illinois at Urbana—Champaign, 1982, Appendix C.
[26] J. D. Kress, Z. Bacic, G. A. Parker, and R. T Pack, Chem. Phys. Lett. **157**, 484–490 (1989).
[27] Z. Bacic, J. D. Kress, G. A. Parker, and R. T Pack, J. Chem. Phys. **92**, 2344–2361 (1990).
[28] J. D. Kress, R. T. Pack, and G. A. Parker, Chem. Phys. Lett. **170**, 306–310 (1990).
[29] F. B. Brown, R. Steckler, D. W. Schwenke, D. G. Truhlar, and B. C. Garrett, J. Chem. Phys. **82**, 188 (1985); R. Steckler, D. G. Truhlar, and B. C. Garrett, *ibid.* **82**, 5499 (1985).